Chemical Engineering Journal 157 (2010) 35–44

Contents lists available at ScienceDirect

Chemical Engineering Journal

journal homepage: www.elsevier.com/locate/cej

Modeling the mineralization and discoloration in colored systems by (US)$Fe^{2+}/H_2O_2/S_2O_8^{2-}$ processes: A proposed degradation pathway

Ivana Grčić*, Dinko Vujević, Natalija Koprivanac

Faculty of Chemical Engineering and Technology, Department of Polymer Engineering and Organic Chemical Technology, University of Zagreb, Marulićev Trg 19, HR-10000, Zagreb, Croatia

ARTICLE INFO

Article history:
Received 13 July 2009
Received in revised form 15 October 2009
Accepted 16 October 2009

Keywords:
Wastewater treatment
Azo dyes
Fenton process
Ultrasound (US)
Mathematical modeling

ABSTRACT

The scope of this experimental research was to study the kinetics of dye mineralization and discoloration in miscellaneous dye systems by advanced Fenton degradation, $Fe^{2+}/H_2O_2/S_2O_8^{2-}$, with and without ultrasound (US) employment. Reactive azo dye C.I. Reactive Violet 2 (RV2) and C.I. Reactive Yellow 3 (RY3) as well as mordant azo dye C.I. Mordant Yellow 10 (MY10) were used as model pollutants for composition of 7 different types of model dye wastewater, i.e. MY10, RV2, RY3, MY10 + RV2, MY10 + RY3, RV2 + RY3 and MY10 + RV2 + RY3 in the concentration of 50 mg L^{-1}. The molar ratio of Fe^{2+}, H_2O_2 and $K_2S_2O_8$ (equimolar) of 1:5 was used, since it was shown as optimal. Mineralization of studied systems was enhanced by simultaneous application of Fenton and US. Mineralization extents obtained after 60 min of treatment varied from minimal 49% for RV2 + RY3 system up to maximal 73% for MY10 + RV2 + RY3 system. Almost 100% of discoloration was achieved in all studied systems within few minutes of applied process. A degradation pathway of studied azo dyes was proposed and 14 variations of mathematical model describing each system and particular process have been developed.

1. Introduction

Wastewaters generated from dye manufacturing and application industries are unacceptable for the receiving water bodies from two main reasons. They are characterised by intensive coloration, so they could affect photosynthetic processes of aquatic plants, reduce oxygen levels in water and in severe cases lead to the suffocation of aquatic flora and fauna in natural recipients. Moreover, the presence of residual dyes and auxiliary chemicals, besides additional loading of the organic content of the recipient, can cause damage to the aquatic life or humans by mutagenic and carcinogenic effects [1]. The overall world's dye production is over 7×10^5 t/year and reactive dyes participate with a large portion. Almost 70% of all reactive dyes are of the azo type [2]. Furthermore, commercial reactive azo dyes are intentionally designed to resist biodegradation [3,4]. It is estimated that 15% of the world's dye production end up in the environment during the manufacturing and application processes [1]. Due to this fact and rapid development and implementation of more and more stringent environmental regulations [5], potential methods for the treatment of this type of wastewater have been under the strong investigation in recent years [6–8]. In general, methods for the colored wastewater treatment can be grouped as biological, physical and chemical ones [9]. Despite to the lot of advantages of biological methods, conventional biological treatment methods are ineffective for degradation of reactive dyes due to their complex aromatic structure and stability. Physical methods of colored wastewater treatment (adsorption, flocculation/coagulation, membrane processes, and ion exchange) [10], generally present transfer of pollution from one phase to the other and they are often expensive and not eco-efficient. Engagement of secondary waste disposal and adsorbents regeneration additionally decreases economical efficiency of these processes. The alternative to the conventional colored wastewater treatment processes presents advanced oxidation processes (AOPs) that can be applied individually or as a part of integral treatment process. The advantage of these processes in comparison with conventional wastewater treatment methods is the possibility of complete degradation of organic load towards water, carbon dioxide, nitrates, sulphates and chlorides. AOPs include formation of highly reactive species (radicals) under the chemical, electrical or radioactive energy and they can react non-selectively with persistent organic compounds transferring them into by-products which can be degraded much more easily [11]. However, AOPs are not suitable for the treatment of heavy loaded industrial wastewater if the concentration of organic compounds exceeds 100–1000 mg C L^{-1} [12] because of the relatively high reactants price. Depending on the free radicals generation; e.g. hydroxyl radical (•OH), with the redox potential of 2.8 eV has the major degradation effect, there are different types of AOPs such as Fenton and Fenton 'like' processes, UV

* Corresponding author. Tel.: +385 1 4597 123; fax: +385 1 4597 143.
E-mail address: igrcic@fkit.hr (I. Grčić).

1385-8947/$ – see front matter © 2009 Elsevier B.V. All rights reserved.
doi:10.1016/j.cej.2009.10.042

photolysis, UV peroxone process, TiO_2 photo-catalysis, high voltage electrical discharge, radiolysis, and sonolysis. Recently, sonochemical degradation of organic dyes has been extensively studied [13] due to advantages such as safety, cleanliness and energy conservation without causing secondary pollution [14,15]. The ultrasonic energy influences the chemical reactions by providing huge heat (pyrolysis) [16] or producing reactive free radicals [17]. The underlying mechanism for a notable effect observed due to ultrasonic irradiation is the cavitation phenomena, which can be defined as formation, growth and subsequent violent collapse of microbubbles or cavities, resulting in the generation of extremely high temperatures and pressures locally, but a millions of such locations in the reactor. The violent collapse of the cavities results in the generation of reactive hydrogen atoms and hydroxyl radicals, leading to formation of hydrogen peroxide and responsible for promoting further oxidation [18]. Although sonochemical reactions could be quite efficient for degradation of organic compounds, it is possible that complete mineralization has not occurred in most cases [19]. This might be due to the higher polarity of the organic compound, low availability of $^{\bullet}OH$ radicals or a lack of dissipated power. To overcome these disadvantages the sonochemical treatment can be combined with AOPs [20,21].

In this study the efficiency of AOPs; advanced (modified) Fenton, $Fe^{2+}/H_2O_2/S_2O_8^{2-}$, and US assisted Fenton processes for degradation of azo dyes C.I. Mordant Yellow 10 (MY10), C.I. Reactive Yellow 3 (RY3) and C.I. Reactive Violet 2 (RV2) in simulated wastewaters was studied. Seven different model dye wastewaters (hereafter: systems); MY10, RV2, RY3, MY10 + RV2, MY10 + RY3, RV2 + RY3, and MY10 + RV2 + RY3, were treated with advanced Fenton process with and without US assistance. The mathematical model describing degradation in each systems and applied process was developed according to the proposed degradation pathway, resulting with 14 variations of the model. The efficiency of each process was evaluated as well.

2. Materials and methods

2.1. Chemicals

All reagents used in this work were analytical reagent grade and used without any further purification. Ferrous sulfate ($FeSO_4{\cdot}7H_2O$), hydrogen peroxide (H_2O_2 30%, w/w), sulphuric acid (H_2SO_4), potassium hydroxide (KOH), potassium peroxodisulfate ($K_2S_2O_8$), sodium thiosulfate ($Na_2S_2O_3{\cdot}10H_2O$), potassium thiocyanate (KSCN), starch and barium chloride ($BaCl_2$) used in this work were supplied by Kemika, Zagreb and ferric sulfate [$Fe_2(SO_4)_3{\cdot}9H_2O$] by Alkaloid, Skopje. Ammonium metavanadate (NH_4VO_3), sodium formate (HCOONa) and *ortho*-phosphoric acid (H_3PO_4 85%) were obtained from Fluka and oxalic acid ($H_2C_2O_4$) was purchased from Sigma–Aldrich. C.I. Reactive Violet 2 (RV2) and C.I. Reactive Yellow 3 (RY3) were obtained from Ciba-Geigy, Switzerland as a free of charge samples. C.I. Mordant Yellow 10 was synthesized in the Laboratory of Ecoengineering, Department of Polymer Engineering and Organic Chemical Technology, Faculty of Chemical Engineering and Technology, University of Zagreb and was characterised by UV/VIS spectrophotometer. The chemical structures and spectral characteristics of dyes studied in this work are presented in Table 1.

2.2. Instruments

A Perkin-Elmer Lambda EZ 201 UV/VIS spectrophotometer was used for discoloration and dearomatization monitoring at λ_{max} = 254, 365, 385 and 550 nm, while mineralization extents were determined on the basis of total organic carbon content measure-

Table 1
Structure and absorptivities of light of studied dyes at wavelengths of maximum absorbance.

Dye	C.I. Mordant Yellow 10 (MY10)		C.I. Reactive Violet 2 (RV2)		C.I. Reactive Yellow 3 (RY3)	
Structure	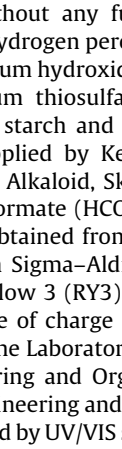		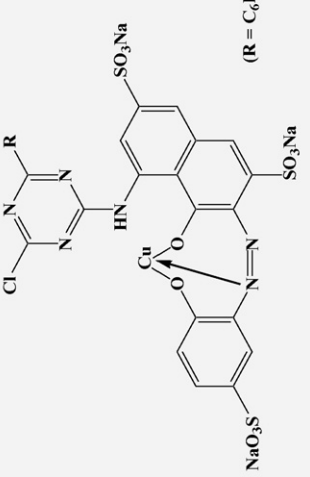 (R = C_6H_5O, NH_2)		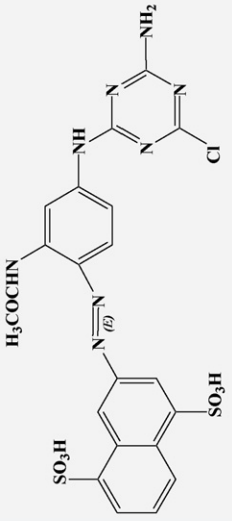	
Molar extinction coefficient (cm^{-1} L mol^{-1})	365 nm	14,400	490		930	
	385 nm	1,055	120		13,000	
	550 nm	0	16,000		0	

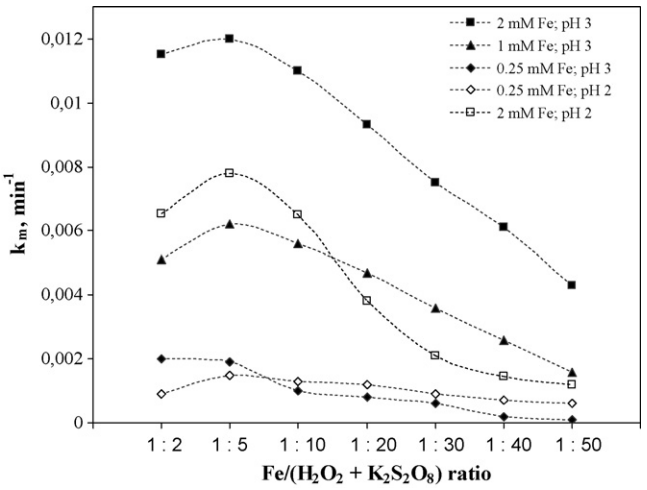

Fig. 1. Influence of different initial process conditions on mineralization rate constant in the system with azo dyes (MY10 + RV2 + RY3) by advanced Fenton process, $Fe^{2+}/H_2O_2/S_2O_8^{2-}$.

ments (TOC), performed by using total organic carbon analyzer; TOC-V_{CPN} 5000 A, Shimadzu. A High Performance Liquid Chromatographer (HPLC), Shimadzu, with SUPELCOGEL H Carbohydrate column, length 250 mm, internal diameter 4.6 mm and UV diode array detector, was used for determination of oxalic acid. Experiments with the employment of ultrasound of 40 kHz (220 V, 50 Hz, 7 A) have been performed in the thermostated ultrasonic bath; a stainless steel tank with bottom-mounted drain, Cole-Parmer, USA. Turbidity of the $BaSO_4$ suspension was measured by Hach 2100 P Turbidimeter (USA).

2.3. Methods

The concentration of each dye was determined on the basis of UV/VIS absorption at λ_{max}, by applying the Lambert–Beer equation to the measured absorbances at their respective λ_{max} and the previously determined absorptivities, shown in Table 1. The system of linear equations was then solved to obtain the concentration of each dye. The concentrations of ferric, ferrous ions and sulfate ions as well as oxalic and other carboxylic acids (fumaric, acetic, malonic and maleic) were determined according to the procedure described in the literature [22]. The content of aromatic compounds and dearomatization extent was determined on the basis of absorbance at 254 nm [23]. Determination of H_2O_2 concentration was based on the reaction of H_2O_2 with ammonium metavanadate [24]. Concentration of cuprous ions was determined by the iodometric method [25].

2.4. Experimental procedure

Experiments were performed as bench scale tests in 120 mL glass reaction vessels with the reaction volume of 100 mL and constant magnetic stirring (600 rpm) or in the ultrasonic bath, at room temperature, 25 ± 3 °C, using 7 different systems i.e. MY10, RV2, RY3, MY10 + RV2, MY10 + RY3, RV2 + RY3 and MY10 + RV2 + RY3, in concentration of 50 mg L^{-1} for each dye. The optimal conditions ($[Fe^{2+}]$ = 2 mM; $[H_2O_2]$ = 5 mM; $[S_2O_8^{2-}]$ = 5 mM; pH 3) were established on the basis of mineralization rate determination as shown in Fig. 1. Apparent mineralization rate constant was presented as a first-order rate constant according to Eq. (1)

$$k_m \times t = -\ln(\mathrm{TOC}_t/\mathrm{TOC}_0) \quad (1)$$

where k_m stands for apparent mineralization rate constant and t stands for time, while TOC_t represents total organic carbon content measured in different periods of time and TOC_0 is initial TOC content in the system.

The initial pH of the studied system was adjusted at 3 using sulphuric acid (c = 1 mol L^{-1}), which was followed by the addition of iron salt, hydrogen peroxide and potassium peroxodisulfate. Samples were taken out in certain periods of time within 60 min; a grain or two of KOH was added in each sample in order to precipitate hydroxides of iron and remove possible absorption interference below 400 nm and then subjected to further analyses.

3. Results and discussion

3.1. Proposed degradation pathway

As presented and discussed in several papers [26–29], degradation of azo dyes can be described by the following stages (Fig. 2): (i) azo bond breakdown that includes lose of saturated character of azo bond and transformation to hydroxyl structure, (ii) tearing the dye molecule (cleavage of –N–N– bond and nitro group formation) when differently substituted aromatic compounds (benzene, naphthalene, and triazine) are produced, (iii) degradation of aromatic rings; naphthalene to benzene, benzene to carboxylic acids, alcohols and aldehydes, with an emphasis on oxalic acid; and oxidation of substituted triazines to cyanuric acid, and finally, (iv) oxidation of oxalic acid to CO_2 by hydroxyl and sulfate radical.

In this work, steps (i) and (ii) were grouped and are presented by (Eq. (2))

$$\begin{matrix}\mathrm{MY10}\\ \mathrm{RV2} + {}^{\bullet}\mathrm{OH} \rightarrow ps\ \mathrm{ArOC}\\ \mathrm{RY3}\end{matrix} \quad (2)$$

Hydroxyl radical is the one responsible for initial breakdown of dye molecules into several differently substituted aromatic compounds. The ArOC abbreviation used in this work accounts for the each aromatic ring, which could be formed after dye molecule breakdown. In the case of RV2, substituted benzene, naphthalene and triazine are the main aromatic compounds. In the case of MY10, there are only two benzene rings left after breakdown. In order to unify a stoichiometry for each system, pseudostoichiometric scheme was proposed based on carbon atom balance (Table 2). Therefore, in presented equations, Eqs. (2)–(4), prefix *ps* stands for stoichiometric coefficient proposed in pseudostoichiometric scheme. Since there are many reactions that could occur in these systems and stoichiometry is not well-determined, proposed scheme is defined as 'pseudo'. For simplification purposes, azo bond breakdown and formation of aromatic compounds were presented by one reaction (Eq. (2)) which rate constant could be varied depending on the studied system (Table 3).

Table 2
Pseudostoichiometric scheme developed on the basis of carbon atom balance.

Simplified model of formation of substituted aromatics and oxalic acid from studied dyes	Corresponding pseudostoichiometric coefficient, ps_i
RV2 or RY3 → 4ArOC → 8 oxalic acid MY10 → 2ArOC → 6 oxalic acid	
Step-by-step reaction	
RV2 or RY3 → ps_1 ArOC	4
ArOC → ps_2 oxalic acid	8
MY10 → ps_3 ArOC	2
ArOC → ps_4 oxalic acid	6
Oxalic acid mineralization	
$(COOH)_2$ → ps_5 CO_2	2

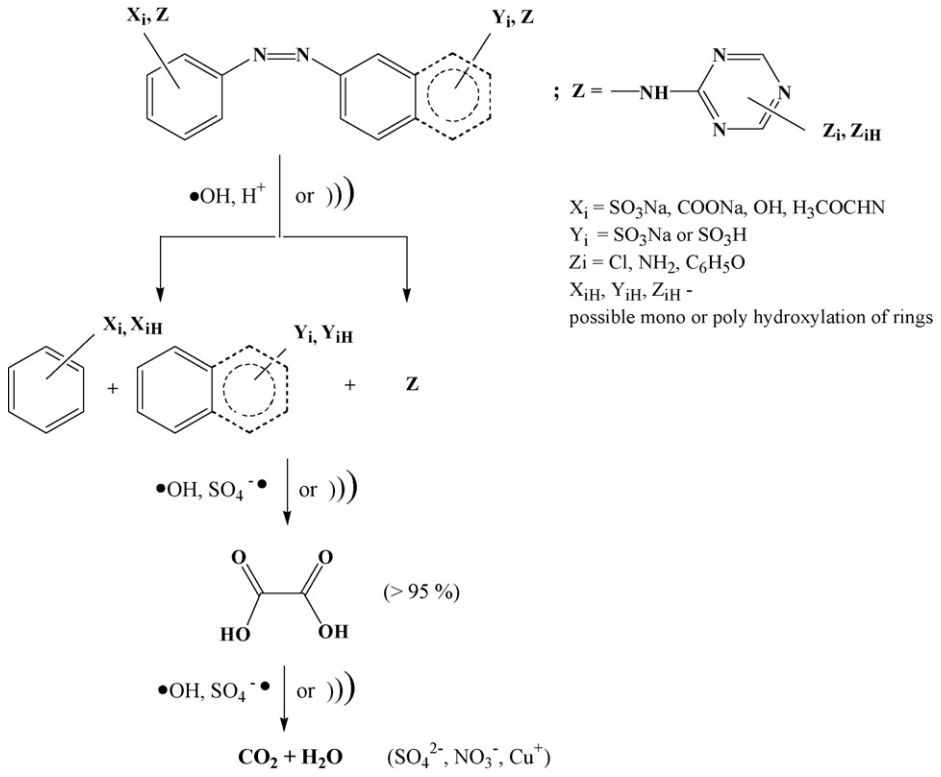

Fig. 2. Proposed degradation pathway.

Also, step (iii) that included ring openings and formation of oxalic acid, was simply presented with the following equations:

$$\beta\text{ArOC} + {}^{\bullet}\text{OH} \rightarrow ps \text{ oxalic acid} \quad (3)$$

$$\beta\text{ArOC} + \text{SO}_4{}^{\bullet -} \rightarrow ps \text{ oxalic acid} \quad (4)$$

As it can be seen, oxalic acid is considered to be a main product [27]. Formation of oxalic acid was confirmed by HPLC analysis. Also, up to 5% max. of other carboxylic acids, i.e. fumaric, acetic, maleic and malonic was detected in fewer cases. Percentage of ArOC which could be degraded by hydroxyl and sulfate radical was given by β, since triazines mainly oxidize only to cyanuric acid [29]. Rate constants of presented reactions could also vary depending on the initial system, i.e. dye. In general, all steps in the reaction mechanism influence the value of reaction rate constant; e.g., in the case where naphthalene compounds exist, this rate constant should include even a degradation of naphthalenes to benzene, i.e. in RV2 and RY3 molecule. Since oxidation of triazines to cyanuric acid is rather slow and consumes a negligible amount of radicals [29], this reaction was not taken into consideration in the overall model.

The presence of inorganic products, else than CO_2, in the treated systems could be addressed to minor amounts of different ions: $SO_4{}^{2-}$, $NO_3{}^{-}$, Cl^{-}, Na^{+}, and Cu^{+}. Composition of treated systems in terms of inorganic ions varies depending on the groups that substitute aromatics within the initial dye structure. For example, degradation of RV2, classified as azo copper complex dye (Table 1), results with simultaneous azo bond breakdown and copper release in the very beginning of applied processes. Amount of cuprous ions remained constant during the treatment. It has been reported that copper has no positive effect on catalysis in similar process system [20]. The presence of copper was not taken into consideration, thus neglected in proposed degradation pathway and model development.

3.2. Model development and rate constants estimation

According to the proposed degradation pathway, representative mathematical model in its 14 variations predicting azo dyes degradation and formation of oxidation products; aromatic compounds and oxalic acid, as well as mineralization of the studied system by the applied processes; $Fe^{2+}/H_2O_2/S_2O_8{}^{2-}$ and $US/Fe^{2+}/H_2O_2/S_2O_8{}^{2-}$, was developed using chemical reactions and rate constants, acquired mostly from the literature [18,30–38]. Reactions accounted for the model development and corresponding rate constants were presented in Table 3. A homogeneous reaction system was assumed.

Regarding the general mass balance for a well-mixed, constant volume and constant temperature batch reactor are given by Eq. (5)

$$r_i = \frac{dc_i}{dt} \quad (5)$$

where c_i is concentration of specie i in the bulk and r_i is the bulk phase rate of the same specie; discoloration and mineralization of dye solutions were simulated by Mathematica 7.0 (Wolfram Research) using GEAR method which finds the numerical solution to the set of ordinary differential equations.

Values of the rate constants for the following reactions: R8–R10, R24, R29–R40 (Table 3) were determined by trial and error method fitting the experimental values into the model (Figs. 3–5). Accuracy of developed model for each system was evaluated by calculating normalized root mean square deviation (NRMSD) as shown in Table 4. A root mean square deviation (RMSD) and normalized one, NRMSD, are presented by Eqs. (6a) and (6b)

$$\text{RMSD} = \sqrt{\frac{1}{N}\sum_{i=1}^{i=N}(y_{e,i} - y_{m,i})^2} \quad (6a)$$

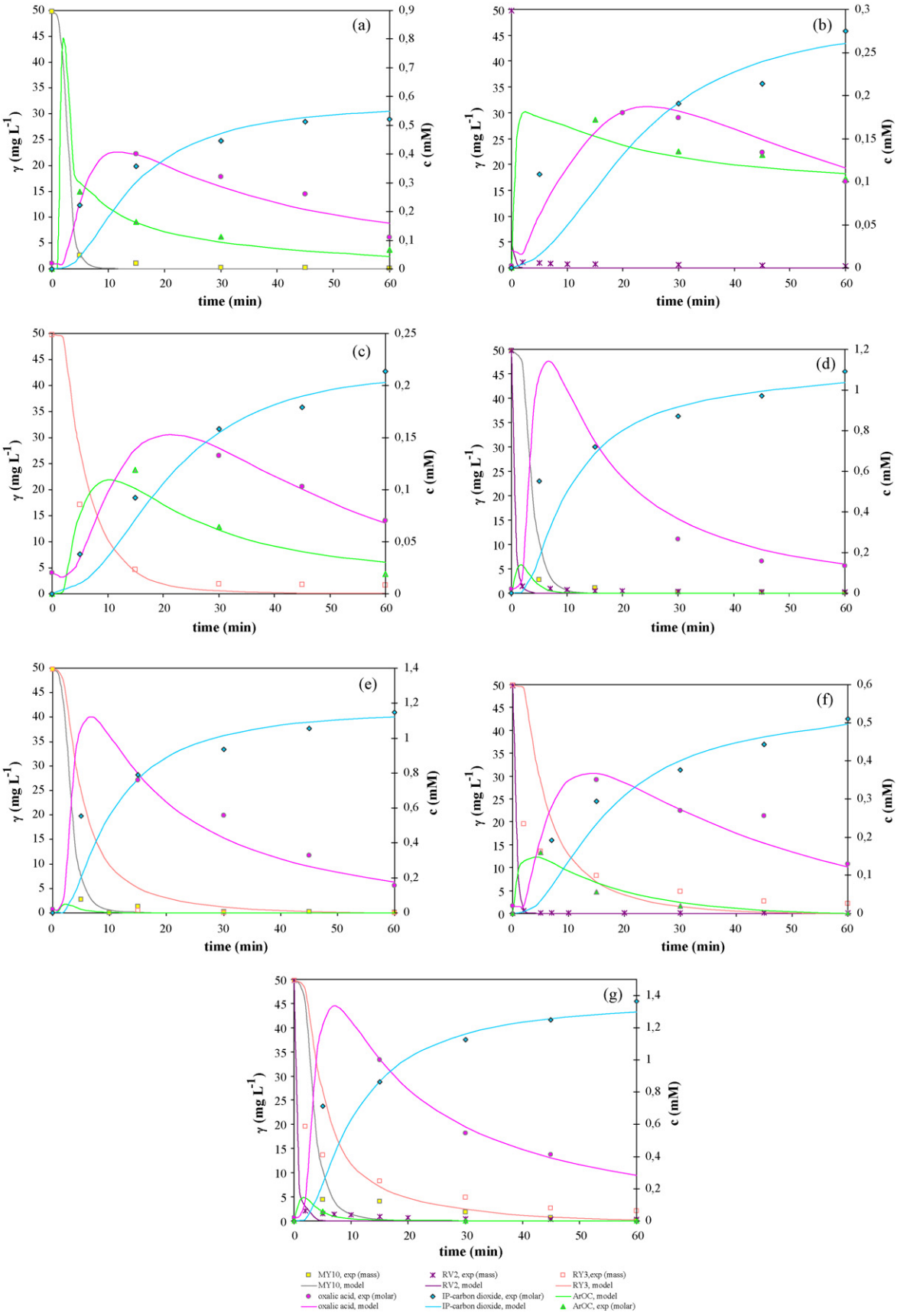

Fig. 3. Model prediction for the degradation of organic compounds in the studied systems by $Fe^{2+}/H_2O_2/S_2O_8^{2-}$ process ($[Fe^{2+}] = 2$ mM; $[H_2O_2] = 5$ mM; $[S_2O_8^{2-}] = 5$ mM; pH 3; $\gamma_{\text{each dye,initial}} = 50\ \text{mg L}^{-1}$); (a) MY10, (b) RV2, (c) RY3, (d) MY10 + RV2, (e) MY10 + RY3, (f) RV2 + RY3 and (g) MY10 + RV2 + RY3.

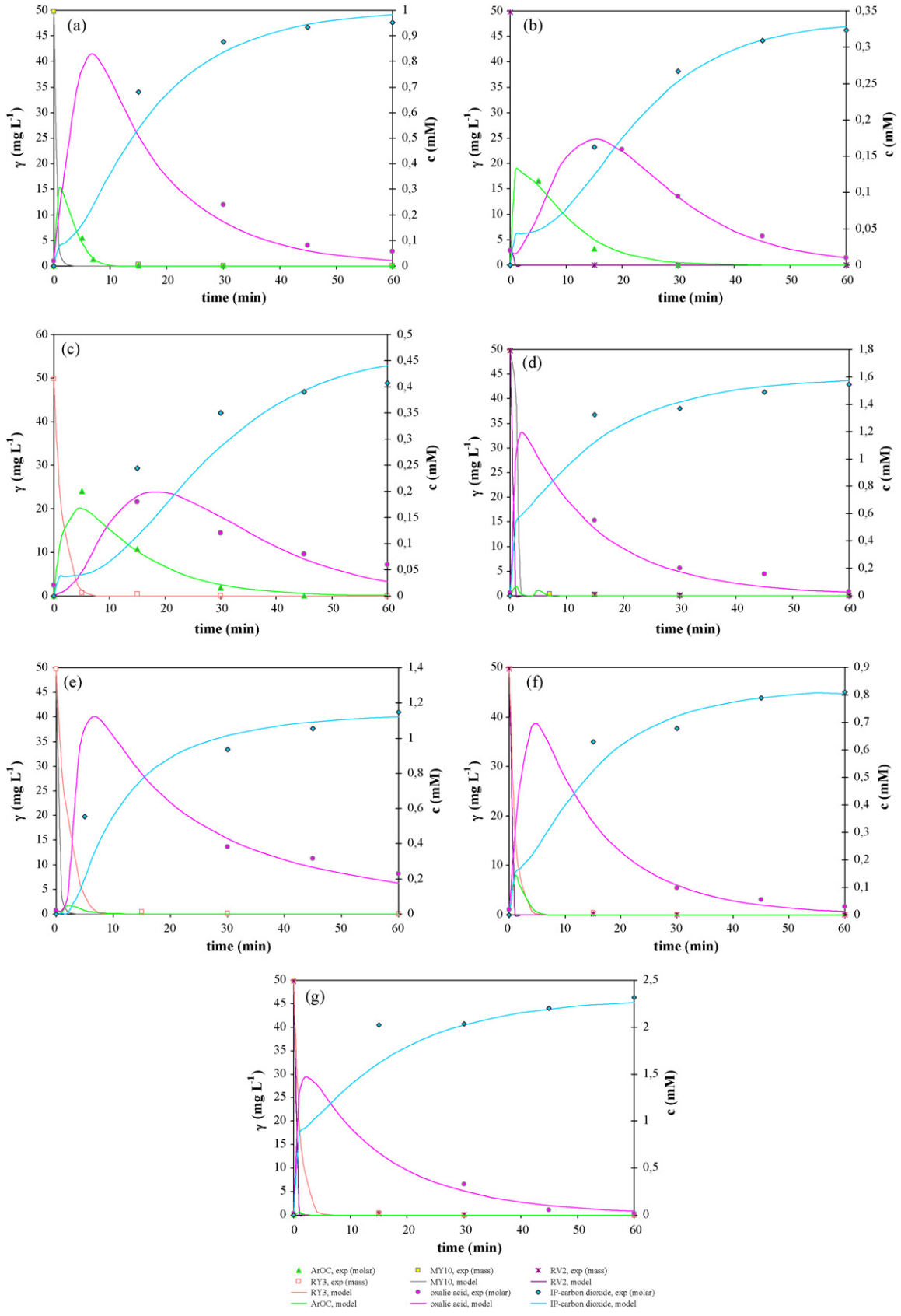

Fig. 4. Model prediction for the degradation of organic compounds in the studied systems by US/Fe^{2+}/H_2O_2/$S_2O_8^{2-}$ process (US: 40 kHz); (a) MY10, (b) RV2, (c) RY3, (d) MY10 + RV2, (e) MY10 + RY3, (f) RV2 + RY3 and (g) MY10 + RV2 + RY3.

Table 3
The reactions and rate constants used for the kinetic modeling; based on homogeneous reaction system.

No.	Reaction	Rate constant ($L\,mol^{-1}\,min^{-1}$)	Reference
Fenton catalytic cycle			
R1	$Fe^{2+} + H_2O_2 \rightarrow Fe^{3+} + OH^{\bullet}$	4560	[30–35]
R2	$Fe^{3+} + H_2O_2 \rightarrow Fe^{2+} + H^+ + HO_2^{\bullet}$	0.6	[30–35]
R3	$Fe^{2+} + OH^{\bullet} \rightarrow Fe^{3+} + OH^-$	1.92×10^{10}	[30–31,35]
R4	$Fe^{2+} + HO_2^{\bullet} \rightarrow Fe^{3+} + H_2O_2$	7.2×10^7	[30–31,35]
R5	$Fe^{3+} + HO_2^{\bullet} \rightarrow Fe^{2+} + H^+ + O_2$	1.86×10^7	[30–31,35]
R6	$Fe^{3+} + O_2^{\bullet -} \rightarrow Fe^{2+} + O_2$	3×10^9	[30–31,35]
R7	$Fe^{2+} + O_2^{\bullet -} \rightarrow Fe^{3+} + H_2O_2$	6×10^8	[30–31,35]
R8	$Fe^{2+} + S_2O_8^{2-} \rightarrow Fe^{3+} + SO_4^{\bullet -} + SO_4^{2-}$	39–49; used 39	This work
R9	$Fe^{3+} + S_2O_8^{2-} \rightarrow Fe^{2+} + 2SO_4^{\bullet -}$	22.5–33.5; used 29.5	This work
R10	$Fe^{2+} + SO_4^{\bullet -} \rightarrow Fe^{3+} + SO_4^{2-}$	1×10^6	This work
Complexes formation			
R11	$Fe^{3+} + H_2O \rightarrow [Fe(OH)]^{2+} + H^+$	1.86×10^{-3}	[30,34]
R12[a]	Fe^{3+} + α-oxalic acid → Fe-oxalate complexes	60	[30,34]
Liquid-phase reactions			
R13	$OH^{\bullet} + H_2O_2 \rightarrow HO_2^{\bullet} + H_2O$	7.2×10^8	[30,31,34]
R14	$2OH^{\bullet} \rightarrow H_2O_2$	3.18×10^{11}	[30,31,34]
R15-1	$H_2O_2 \rightarrow HO_2^- + H^+$	2.22	[30,31]
R15-2	$HO_2^- + H+ \rightarrow H_2O_2$	1.56×10^{12}	[30,31]
R16	$OH^{\bullet} + HO_2^- \rightarrow HO_2^{\bullet} + H_2O$	4.5×10^{11}	[30,31,34]
R17	$OH^{\bullet} + HO_2^{\bullet} \rightarrow H_2O + O_2$	3.96×10^{11}	[30,31,34]
R18	$2HO_2^{\bullet} \rightarrow H_2O_2 + O_2$	4.98×10^7	[30,31,34]
R19	$HO_2^{\bullet} \rightarrow O_2^{\bullet -} + H^+$	$9.48 \times 10^6\ min^{-1}$	[30,31,34]
R20	$OH^{\bullet} + H_2O_2 \rightarrow O_2^{\bullet -} + H_2O$	1.62×10^9	[30,31,34]
R21	$HO_2^{\bullet} + O_2^{\bullet -} \rightarrow HO_2- + O_2$	5.82×10^9	[30,31,34]
R22	$OH^{\bullet} + O_2^{\bullet -} \rightarrow O_2 + OH^-$	4.2×10^{11}	[30,31,34]
R23	$O_2^{\bullet -} + H^+ \rightarrow HO_2^{\bullet}$	6×10^{11}	[30,31]
R24-1	$SO_4^{\bullet -} + H_2O \rightarrow HO^{\bullet} + H^+ + SO_4^{2-}$	6.3×10^7	This work
R24-2	$SO_4^{2-} + {}^{\bullet}OH \rightarrow SO_4^{\bullet -} + OH^-$	1.5×10^8	This work
Ultrasonic induced radical formation[b]			
R25	$H_2O \xrightarrow{)))} H^{\bullet} + OH^{\bullet}$	$2 \times 10^{-5}\ min^{-1}$	[38]
R26	$H^{\bullet} + O_2 \rightarrow HO_2^{\bullet}$	1×10^{11}	This work
R27	$H_2O_2 \xrightarrow{)))} 2OH^{\bullet}$	$0.7\ min^{-1}$	[38]
R28	$S_2O_8^{2-} \xrightarrow{)))} 2SO_4^{\bullet}-$	$5 \times 10^2\ min^{-1}$	[37]
Degradation of pollutants			
R29	RV2 + $OH^{\bullet}$ → *ps* ArOC	7.2×10^{11}	This work
R30	RY3 + $OH^{\bullet}$ → *ps* ArOC	$(1.5–2.4) \times 10^9$	This work
R31	MY10 + $OH^{\bullet}$ → *ps* ArOC	$(6–6.6) \times 10^9$	this work
R32[c]	β ArOC + $OH^{\bullet}$ → *ps* oxalic acid; $\beta = 0.75$ or 1	$1 \times (10^7–10^{10})$	This work [36]
R33	β ArOC + $SO_4^{\bullet -}$ → oxalic acid	$1.2 \times 10^4–7.2 \times 10^6$	This work
R34[d]	$(1-\alpha)$ oxalic acid + $OH^{\bullet}$ → IP (*ps* $CO_2 + H_2O$)	1.8×10^7	This work [36]
R35	$(1-\alpha)$ oxalic acid + $SO_4^{\bullet -}$ → IP (*ps* $CO_2 + H_2O$)	3×10^{10}	This work
R36	RV2 $\xrightarrow{)))}$ *ps* ArOC	$9.8 \times 10^{-3}\ min^{-1}$	This work
R37	RY3 $\xrightarrow{)))}$ *ps* ArOC	$5 \times (10^{-5}–10^{-4})\ min^{-1}$	This work
R38	MY10 $\xrightarrow{)))}$ *ps* ArOC	$7.2 \times 10^{-3}\ min^{-1}$	This work
R39	(β) ArOC $\xrightarrow{)))}$ *ps* oxalic acid	$(1.2 \times 10^{-5}–9 \times 10^{-4})\ min^{-1}$	This work [18]
R40	$(1-\alpha)$ oxalic acid $\xrightarrow{)))}$ IP ($CO_2 + H_2O$)	$3.16 \times 10^{-2}\ min^{-1}$	This work

[a] Part of oxalic acid that involves in complexation with Fe^{3+} is set at 50%, i.e. $\alpha = 0.5$.
[b] Reaction nos. 14 and 18 are also included in sonochemical decomposition cycle; therefore in systems with ultrasonic assistance, rates for these reactions were duplicated.
[c] In systems with RV2 and RY3 only non-triazinic aromatics react according to reactions nos. 32, 33 and 39; in that case, β was set to 0.75.
[d] IP stands for inorganic products; for modeling purposes IP was equalized to amount of CO_2 formed.

$$\mathrm{NRMSD} = \frac{\mathrm{RMSD}}{y_{\max} - y_{\min}} \tag{6b}$$

where N represents number of data points, y_e stands for observed value and y_m for the value predicted by the model. RMSD and NRMSD are frequently used measures of differences between values predicted by a model and the values observed, i.e. obtained by experiment. NRMSD is considered to be a good measure of accuracy [39,40].

As it can be seen from Table 4, NRMSD calculated for each response, concentration of dyes, concentration of aromatic compounds, oxalic acid and CO_2, point out a slight difference between values obtained by model with the ones observed experimentally, suggesting the model is accurate. For the system containing all the three model dyes (MY10 + RV2 + RY3), additional responses were taken into account; concentration of hydrogen peroxide, ferrous and ferric ions, sulfate ions as well as pH value. NRMSDs calculated for these responses also show good match between model and experiment (Table 4). It can be concluded that data support a proposed degradation pathway and model assumptions.

When discussing the model, it has to be pointed out that some of the reactions; R32, R34 and R39, were collated with similar ones found in the literature, approved as a useful in rate constants estimation. The reactions within Fenton catalytic cycle, i.e. reactions between ferrous and ferric ions with peroxodisulfate anions, R8 and R9, were found to be slow, therefore dictating the overall degrada-

Table 4
Normalized root mean square deviations (NRMSD) for the evaluation of model accuracy.

Process	$Fe^{2+}/H_2O_2/S_2O_8^{2-}$							$US/Fe^{2+}/H_2O_2/S_2O_8^{2-}$						
System	MY10	RV2	RY3	MY10 + RV2	MY10 + RY3	RV2 + RY3	MY10 + RV2 + RY3	MY10	RV2	RY3	MY10 + RV2	MY10 + RY3	RV2 + RY3	MY10 + RV2 + RY3
NRMSDs														
γ(MY10)	0.0095	–	–	0.0895	0.0375	–	0.0614	0.0019	–	–	0.0019	0.0019	–	0.0019
γ(RV2)	–	0.0139	–	0.0097	–	0.0026	<0.0001	–	<0.0001	–	0.0021	–	0.0021	0.0021
γ(RY3)	–	–	0.0867	–	0.0484	0.0557	0.0877	–	–	0.0062	–	0.0044	0.0044	0.0044
[ArOC]	0.0193	0.0116	0.0106	<0.0001	<0.0001	<0.0001	<0.0001	0.0084	0.00874	0.0154	<0.0001	<0.0001	<0.0001	<0.0001
[Oxalic]	0.0433	0.0104	0.0037	0.1678	0.0679	0.0330	0.0231	0.0390	0.0037	0.0231	0.0479	0.0434	0.0143	0.0455
	0.0786	0.0440	0.0155	0.1443	0.1429	0.0849	0.1458	0.0672	0.0182	0.0666	0.0646	0.1429	0.0502	0.0721
$[H_2O_2]$	–		–				0.0679							0.0393
pH							0.0202							0.0245
$[Fe^{2+}]$							0.0319							0.0287
$[Fe^{3+}]$							0.0706							0.0553
$[SO_4^{2-}]$							0.0071							0.0135

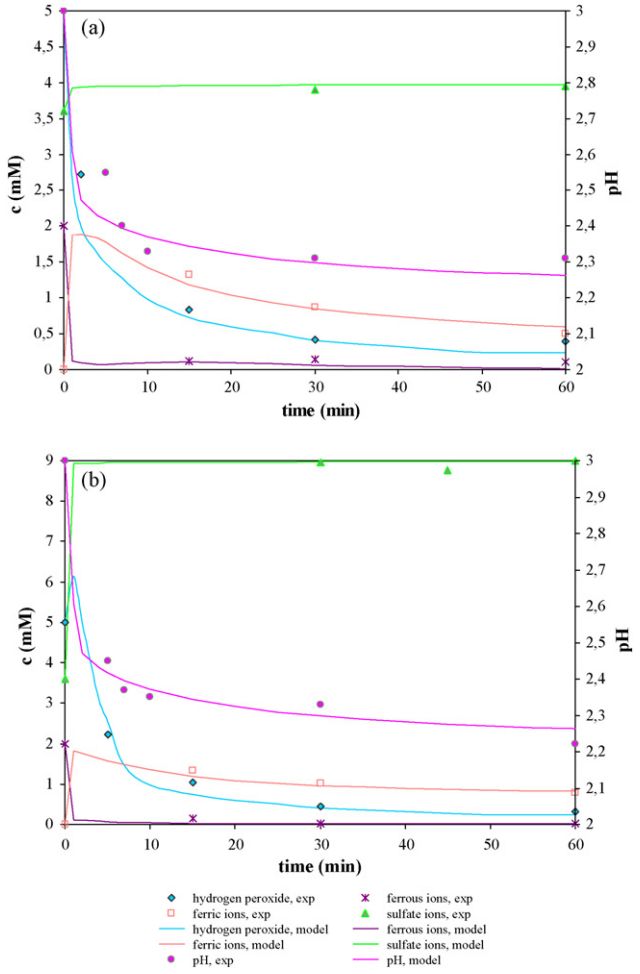

Fig. 5. Model prediction for the H_2O_2 consumption, SO_4^{2-} formation and changes in Fe^{2+}, Fe^{3+}, H^+ (pH) concentrations, during the process: (a) $Fe^{2+}/H_2O_2/S_2O_8^{2-}$ and (b) $US/Fe^{2+}/H_2O_2/S_2O_8^{2-}$.

tion rate in great extent. This observation is in accordance with classical Fenton reaction cycle. Namely, reactions of ferrous and ferric ions with hydrogen peroxide (R1 and R2) are the limiting ones [30]. Rate constants for the reactions that considered employment of ultrasound, particularly cavitation, R36–R40, are actually pseudo-constants since their values integrated all the influences on the cavitational phenomena. These pseudo-constants include influence of temperature, gas (air) content in the solution, solution level and ultrasound power [41]. In the studied systems mentioned constants are valid since they are estimated for particular configuration of reaction system at ambiental conditions. All experiments were performed at room temperature with oscillation of ±3 °C. It was important to keep temperature constant since cavitation depends on it. If temperature rises, bubbles in the solution would become more numerous and cavitation should be more intensive. On the other hand, as the temperature rises, liquid has a higher vapor pressure and gas content in the bubbles becomes higher and the intensity of cavitation collapse decreases. To comply with these two opposing effects, experiments should be performed in the range from 20 to 45 °C [41]. In this work, experimental data obtained when ultrasound was employed is representative, as ensured by choosing the operating temperature within the optimal range.

A potential binding of copper, released after azo bond breakdown in RV2 molecule (Section 3.1), with triazinic compounds was not taken into account since copper concentration remains constant during the each process. Possible catalytic activity of copper

was also neglected according to the previous researches [20,42]. As it can be seen from Table 3, IP is equalized with CO_2 concentration. Formation of other IPs (SO_4^{2-}, NO_3^-, Cl^-, Na^+, and Cu^+), as a final product of aqueous inorganics oxidation in the system is included in reactions R29–R33 and R36–R39, influencing the value of reaction rate constant. For the example, when azo bond splits, nitro groups are formed instantly, and, in the case of RV2, cuprous ions are released simultaneously.

From the results presented with Fig. 3a it can be seen that degradation of MY10 up to the ArOC occurred in a first few minutes of the process. Also, it can be observed that the amount of the formed ArOC was significantly higher than in other studied systems (Fig. 3b–f). That can be explained by the chemical structure of the studied dyes (Table 1). Namely, due to the more complex structure of RV2 and RY3 in comparison with MY10, a larger amount of organic radicals that participate in degradation pathway were formed. On the other hand, in the case of simultaneous application of Fenton and US it can be observed that the lower amount of ArOC was formed in all the studied systems (Fig. 4a–f), implying once again that US enhances dye degradation pathway over oxalic acid to the complete mineralization.

Regarding the rates of formation and consequent degradation of aromatic compounds in the studied systems, ArOCs, R30–R33, R37–R39 (Table 3), an interesting observation can be stated; rate constants vary depending on the system, attaining higher values, even 1×10^{10} L mol^{-1} min^{-1}, as system becomes more complex. This can be explained by the following: (i) the enhanced intensity of cavitation [43] and (ii) a formation of a wide range of different organic radicals, resulting with numerous shifting of unpaired electrons, and, eventually, with higher degradation extent, e.g., organic peroxide radical could be formed. Although, they are usually neglected in the model development [30], there is still a certain influence of these and other organic radicals on overall degradation, since proposed degradation pathway (Fig. 2) assumed a free radical mechanism.

3.3. Evaluation of the process efficiency

The optimal conditions ($[Fe^{2+}] = 2$ mM; $[H_2O_2] = 5$ mM; $[S_2O_8^{2-}] = 5$ mM; pH 3) were established on the basis of determined mineralization rate constants as previously stated (Fig. 1). The main idea was to combine two oxidants in order to achieve better mineralization extent due to consequent generation of different nonselective radicals, $^{\bullet}OH$, $S_2O_8^{\bullet -}$ and $SO_4^{\bullet -}$. By implementing this approach it is also possible to overcome disadvantages of each oxidant, such as stability of H_2O_2 and the usage of large amounts of peroxodisulfate salts that may result with high concentration of sulfate ions in a treated water.

Based on past experience [22], ferrous sulfate was chosen as the most appropriate reagent for the Fenton application. Furthermore, pH 3 was selected as optimal pH condition [44]. As pH was adjusted using H_2SO_4, a respective amount of sulfate ions was present at the beginning of the each process (3.6 mM, Fig. 5). According to the reaction R24–2 (Table 3), this initial amount of sulfate ions in the system leads to a generation of additional amount of sulfate radicals, somewhat responsible for the propagation of ArOCs and oxalic acid oxidation by a free radical mechanism.

As it can be seen (Fig. 6), TOC content was reduced in higher extent when ultrasound (US) was involved in advanced Fenton process, although US alone resulted in low mineralization extent. This can be explained by the fact that US allows better homogenization of the system, i.e. more effective mass transfer that could be compared with well-mixing. Furthermore, US waves induce a bubble collapse [17,18]. In this micro-bubbles, conditions are extreme (5000 K, 500 atm) and reactions in it should be very fast. Also, outside the bubble, water molecules are decomposed and radicals are

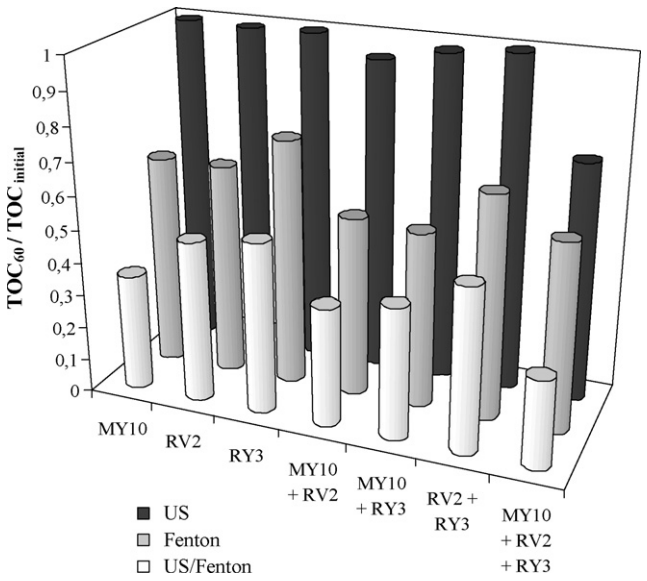

Fig. 6. Overall mineralization extent achieved by applied processes after 60 min.

formed (R14, R18, R25–R28, Table 3). So, this additional amount of radicals, as well as additional amount of hydrogen peroxide should improve efficiency of the overall process. However, as model predicted (Fig. 5b), the burst of H_2O_2 production occurred in the very beginning of the process, which could result with high mineralization extent in the first minute. This can be observed from Fig. 4, where a large amount of CO_2 was produced in the systems. Degradation of organic compounds, dyes, aromatic products and oxalic acid, caused by ultrasonic waves, i.e. cavitation, occurs continuously in the studied systems (R36–R40).

The most interesting result is the notable minimization of TOC content in miscellaneous dye systems (Fig. 6). This is particularly emphasized when only US was used for dye degradation, where 30% of mineralization was achieved in the system containing all three model dyes (MY10 + RV2 + RY3). Theory of cavitation offered a reasonable explanation. Although the cavitation threshold as a function of dissolved species is not straightforward, as the concentration of dissolved species increases, the threshold also increases, relative to low concentrations [43]. On the other hand, increasing the cavitational threshold intensity increases once cavitation is reached, so the more difficult it is to produce cavitation, the higher the intensity will be. In presented case, three different dye molecules are dissolved in water at relatively low concentration (50 mg L^{-1} each). According to the theory of cavitation, increasing the concentration of dissolved dyes, i.e. increasing the number of molecules in the system, intensity of cavitation would be higher due to increasing the cavitational threshold. The observed phenomenon could also be explained by the formation of organic radicals and their influence on the overall degradation (Section 3.2).

4. Conclusions

The mineralization and discoloration of MY10, RV2 and RY3 in 7 different model dye wastewaters by advanced Fenton oxidation with and without employment of US were studied. It has been found out that engagement of ultrasonic energy enhances overall process efficiency significantly. Mineralization extents achieved after 60 min of the treatment were as follows: 65% for MY10, 51% for RV2, 48% for RY3, 64% for MY10 + RV2, 60% for MY10 + RY3, 49% for RV2 + RY3 and 73% for MY10 + RV2 + RY3 model dye wastewater system. Almost 100% of discoloration of all studied dye systems was achieved even in a few minutes of applied process. A degra-

dation pathway for azo dyes was proposed, and consequently, 14 variations of the representative mathematical model describing mineralization and discoloration were developed. This model fits the series of experimental data satisfactory in all the studied systems and for both applied processes. NRMSDs, as a measure of error, were calculated to evaluate the accuracy of developed model for each observed response in each system. In some systems, NRMSD for concentration of RV2 is very low, even below 0.0001, but usually around 0.0020. Concentration of aromatic compounds as a function of time is best described by a developed model, e.g., NRMSD for [ArOC] are often about 0.0001. The most obvious is the difference between predicted and observed values for CO_2, where NRMSD is found to be up to 0.1458 referring to mineralization in the complex system MY10 + RV2 + RY3 by modified Fenton process, $Fe^{2+}/H_2O_2/S_2O_8{}^{2-}$. Finally, all observations made on the basis of achieved results and model predictions, confirmed a proposed degradation pathway based on free radicals mechanism as well as the assumptions made for model development.

Acknowledgements

We would like to acknowledge the financial support from the Croatian Ministry of Science, Education and Sport, Project #125-1253092-1981. Also, we would like to express our gratitude to Dr Gordana Matijašić, assistant professor at Faculty of Chemical Engineering and Technology, University of Zagreb, for providing the ultrasonic bath used in this work.

References

[1] R. Nilsson, R. Nordlinder, U. Wass, B. Meding, L. Belin, Asthma, rhinitis, and dermatitis in workers exposed to reactive dyes, Br. J. Ind. Med. 50 (1993) 65–70.
[2] I. Arslan, A.I. Balcioglu, T. Tuhkanen, Advanced oxidation of synthetic dyehouse effluent by O_3, H_2O_2/O_3 and H_2O_2/UV processes, Environ. Tech. 20 (1999) 921–931.
[3] M.S. Lucas, A.A. Dias, A. Sampaio, C. Amaral, J.A. Peres, Degradation of a textile reactive Azo dye by a combined chemical–biological process: Fenton's reagent–yeast, Water Res. 41 (2007) 1103–1109.
[4] W. Jing, L. Lihua, Z. Jiti, L. Hong, L. Guangfei, J. Ruofei, Y. Fenglin, Enhanced biodecolorization of azo dyes by electropolymerization-immobilized redox mediator, J. Hazard. Mater. 168 (2009) 1098–1104.
[5] C. Hessel, C. Allegre, M. Maisseu, F. Charbit, P. Moulin, Guidelines and legislation for dye house effluents, J. Environ. Manage. 83 (2007) 171–180.
[6] J.M. Chacón, M.T. Leal, M. Sánchez, E.R. Bandala, Solar photocatalytic degradation of azo-dyes by photo-Fenton process, Dyes Pigm. 69 (2006) 144–150.
[7] T. Robinson, G. McMullan, R. Marchant, P. Niagam, Remediation of dyes in textile effluent: a critical review on current treatment technologies with a proposed alternative, Bioresour. Technol. 77 (2001) 247–255.
[8] E. Forgas, T. Cserháti, G. Oros, Removal of synthetic dyes from wastewaters: a review, Environ. Int. 30 (2004) 953–971.
[9] R.S. Gupta, Environmental Engineering and Science, An Introduction, Government Institutes, Rockville, 1997.
[10] P.K. Malik, S.K. Sanyal, Kinetics of decolourisation of azo dyes in wastewater by UV/H_2O_2 process, Sep. Purif. Technol. 36 (2004) 167–175.
[11] J.H. Ramirez, C.A. Costa, L.M. Madeira, Experimental design to optimize the degradation of the synthetic dye Orange II using Fenton's reagent, Catal. Today (2005) 107–108.
[12] M. Muruganandham, M. Swaminathan, Decolourisation of Reactive Orange 4 by Fenton and photo-Fenton oxidation technology, Dyes Pigm. 63 (2004) 315–321.
[13] P. Chowdhury, T. Viraraghavan, Sonochemical degradation of chlorinated organic compounds, phenolic compounds and organic dyes—a review, Sci. Total Environ. 407 (2009) 2474–2492.
[14] K.C. Teo, Y. Xu, C. Yang, Sonochemical degradation for toxic halogenated organic compounds, Ultrason. Sonochem. 8 (2001) 241–246.
[15] H. Hao, M. Wu, Y. Chen, Y. Yin, Z. Lu, Cavitation-induced pyrolysis of toxic chlorophenol by high frequency ultrasonic irradiation, Wiley Periodicals, Inc., Environ. Toxicol. 18 (2003) 413–417.
[16] K.Y. Kim, K. Byun, H. Kwak, Temperature and pressure fields due to collapsing bubble under ultrasound, Chem. Eng. J. 132 (2007) 125–135.
[17] K.S. Suslick, The chemical effect of ultrasound, Sci. Am. 260 (1989) 80–86.
[18] P.R. Gogate, S. Mujumdar, A.B. Pandit, Sonochemical reactors for waste water treatment: comparison using formic acid degradation as a model reaction, Adv. Environ. Res. 7 (2003) 283–299.
[19] V. Desai, M.A. Shenoy, P.R. Gogate, Degradation of polypropylene using ultrasound-induced acoustic cavitation, Chem. Eng. J. 140 (2008) 483–487.
[20] A.G. Chakinala, P.R. Gogate, A.E. Burgess, D.H. Bremmer, Industrial wastewater treatment using hydrodynamic cavitation and heterogeneous advanced Fenton processing, Chem. Eng. J. 152 (2009) 498–502.
[21] H. Zhang, Y. Lv, F. Liu, D. Zhang, C.I. Degradation of, Acid Orange 7 by ultrasound enhanced ozonation in a rectangular air-lift reactor, Chem. Eng. J. 138 (2008) 13–18.
[22] I. Grčić, D. Vujević, J. Šepčić, N. Koprivanac, Minimization of organic content in simulated industrial wastewater by Fenton type processes: A case study, J. Hazard. Mater. 170 (2009) 954–961.
[23] APHA, Standard Methods for the Examination of Water and Wastewater Treatment, 20th ed., American Public Health Association, Washington, DC, USA, 1998.
[24] R.F.P. Nogueira, M.C. Oliveira, W.C. Paterlini, Simple and fast spectrophotometric determination of H_2O_2 in photo-Fenton reactions using metavanadate, Talanta 66 (2005) 86–91.
[25] E.W. Hammock, E.H. Swift, Iodometric determination of copper. Effect of thiocyanate on end point and use of sulfate–hydrogen sulfate buffers, Anal. Chem. 21 (1949) 975–980.
[26] E. Pramauro, A. Bianco Prevot, M. Vincenti, R. Gamberini, Photocatalytic degradation of naphthalene in aqueous TiO_2 dispersions: effect of nonionic surfactants, Chemosphere 36 (1998) 1523–1542.
[27] A.N.M. Bagyo, W. Andayani, H. Winarno, E. Katrin, Y.S. Soebianto, Radiolysis of reactive azo dyes in aqueous solution, Atom Indonesia 30 (2004) 45–51.
[28] A. Gutowska, J. Kałużna-Czaplińska, W.K. Jóźwiak, Degradation mechanism of Reactive Orange 113 dye by H_2O_2/Fe^{2+} and ozone in aqueous solution, Dyes Pigm. 74 (2007) 41–46.
[29] J. García-Montaño, F. Torrades, L.A. Pérez-Estrada, I. Oller, S. Malato, M.I. Maldonado, J. Peral, Degradation pathways of the commercial reactive Azo Dye Procion Red H-E7B under solar-assisted photo-Fenton reaction, Environ. Sci. Technol. 42 (2008) 6663–6670.
[30] N. Kang, D.S. Lee, J. Yoon, Kinetic modeling of Fenton oxidation of phenol and monochlorophenols, Chemosphere 47 (2002) 915–924.
[31] H. Gallard, J. De Laat, Kinetic modelling of Fe(III)/H_2 O_2 oxidation reactions in dilute aqueous solution using atrazine as a model organic compound, Water Res. 34 (12) (2000) 3107–3116.
[32] J.C. Crittenden, S. Hu, D.W. Hand, S.A. Green, A kinetic model for H_2O_2/UV process in a completely mixed batch reactor, Water Res. 33 (10) (1999) 2315–2328.
[33] A.A. Burbano, D.D. Dionysiou, M.T. Suidan, T.L. Richardson, Oxidation kinetics and effect of pH on the degradation of MTBE with Fenton reagent, Water Res. 39 (2005) 107–118.
[34] H. Kušić, N. Koprivanac, A. Lončarić Božić, I. Selanec, Photo-assisted Fenton type processes for the degradation of phenol: a kinetic study, J. Hazard. Mater. B136 (2006) 632–644.
[35] R. Andreozzi, A. D'Apuzzo, R. Marotta, A kinetic model for the degradation of benzothiazole by Fe^{3+}-photo-assisted Fenton process in a completely mixed batch reactor, J. Hazard. Mater. B80 (2000) 241–257.
[36] M.A. Tarr, Chemical Degradation Methods for Wastes and Pollutants—Environmental and Industrial Applications, Marcel Dekker Inc., New York, USA, 2003.
[37] G.J. Price, A.A. Clifton, Sonochemical acceleration of persulfate decomposition, Polymer 37 (1996) 3971–3973.
[38] K. Okitsu, K. Iwasaki, Y. Yobiko, H. Bandow, R. Nishimura, Y. Maeda, Sonochemical degradation of azo dyes in aqueous solution: a new heterogeneous kinetics model taking into account the local concentration of OH radicals and azo dyes, Ultrason. Sonochem. 12 (2005) 255–262.
[39] E.A. Coutsias, C. Seok, K.A. Dill, Using quaternions to calculate RMSD, J. Comput. Chem. 25 (2004) 1849–1857.
[40] W. Kabsch, A solution for the best rotation to relate two sets of vectors, Acta Cryst. A 32 (1976) 922–923.
[41] B. Niemczewski, Observations of water cavitation intensity under practical ultrasonic cleaning conditions, Ultrason. Sonochem. 14 (2007) 13–18.
[42] I. Grčić, M. Mužic, D. Vujević, N. Koprivanac, Evaluation of atrazine degradation in UV/FeZSM-5/H_2O_2 system using factorial experimental design, Chem. Eng. J. 150 (2009) 476–484.
[43] M.A. Margulis, Sonochemistry and Cavitation, Gordon and Breach Science Publishers, Luxembourg, 1995.
[44] B. Muthukumari, K. Selvam, I. Muthuvel, M. Swaminathan, Photoassisted hetero-Fenton mineralisation of azo dyes by Fe(II)–Al_2O_3 catalyst, Chem. Eng. J. 153 (2009) 9–15.